Available online www.jocpr.com

Journal of Chemical and Pharmaceutical Research, 2014, 6(10):528-535

Research Article

ISSN : 0975-7384
CODEN(USA) : JCPRC5

Binding modes study on enantiomers of BYK 311319 as potassium-competitive acid blockers

Xing-Xing Xian-Yu[1], Cong Wu[1], Hua-Jun Luo[1*] and Wei-Qiao Deng[2]

[1]College of Biological and Pharmaceutical Science, China Three Gorges University, Yichang, China
[2]Dalian Institute of Chemical Physics, Chinese Academy of Sciences, Dalian, China

---

ABSTRACT

Potassium-competitive acid blocker (9S)-BYK 311319 (pIC_{50}=6.8) showed significantly higher inhibition activity than (9R)-enantiomer (pIC_{50}=5.4). Here the binding modes of BYK 311319 enantiomers with H^+,K^+-ATPase were studied by Homology modeling, induced-fit docking (IFD), molecular dynamics and MM/GBSA calculation methods. The docking Gscores, IFD scores and ΔG_{bind} (binding free energies) of (9S)-BYK 311319 (-9.64, -1724.74 and -47.71 kcal/mol) are more favorable than those of (9R)-enantiomer (-6.98, -1723.88 and -43.14 kcal/mol), which is consistent with the experimental inhibition activities. (9S)-BYK 311319 has hydrogen bond interaction with the key residue Cys813 and interacts with residues Gln127, Thr135, Asp136, Asp137 and Asn138 in the TM1-2 loop of H^+,K^+-ATPase through charged interactions.

Keywords: BYK 311319; enantiomers; Potassium-competitive acid blocker; induced-fit docking; binding free energy

---

INTRODUCTION

Peptic ulcer diseases, such as gastric ulcers and gastro esophageal reflux disease (GERD), are chronic inflammation of the stomach and duodenum and strongly influence the life quality of the patients [1-3]. Proton pump (H^+,K^+-ATPase) inhibitors (PPIs) such as omeprazole, lansoprazole, rabeprazole, pantoprazole, tenatoprazole and leminoprazole are considered as the first-line therapy for acid suppression [4]. But primarily due to their chemical structures and irreversible inhibition of H^+,K^+-ATPase, PPIs exhibit a delayed onset of acute effect and achieve full effect only slowly [5]. Now a new class of H^+,K^+-ATPase reversible inhibitors designated as potassium-competitive acid blockers (P-CABs) could offer some therapeutic advantages by competing with the K^+ on the luminal surface and provide faster onset and longer duration of action than conventional PPIs [5].

SCH 28080 (Fig. 1) is the first clinical research P-CAB and shows excellent antisecretory and cytoprotective properties [6]. However, because of extensive metabolism and associated liver toxicity, the clinical development of SCH 28080 was stopped [7]. Then some chemical analogues of SCH 28080 such as BYK 311319 (Fig. 1) were synthesized [8]. Andreas Marc Palmer *et al.* reported [8, 9] that the (9S)-BYK 311319 (pIC_{50}=6.8) showed significantly higher biological activity than (9R)-enantiomer (pIC_{50}=5.4) [9]. So in this paper, it is interesting to study the binding modes of BYK 311319 enantiomers with H^+,K^+-ATPase by molecular docking, molecular dynamics and MM/GBSA calculation methods.

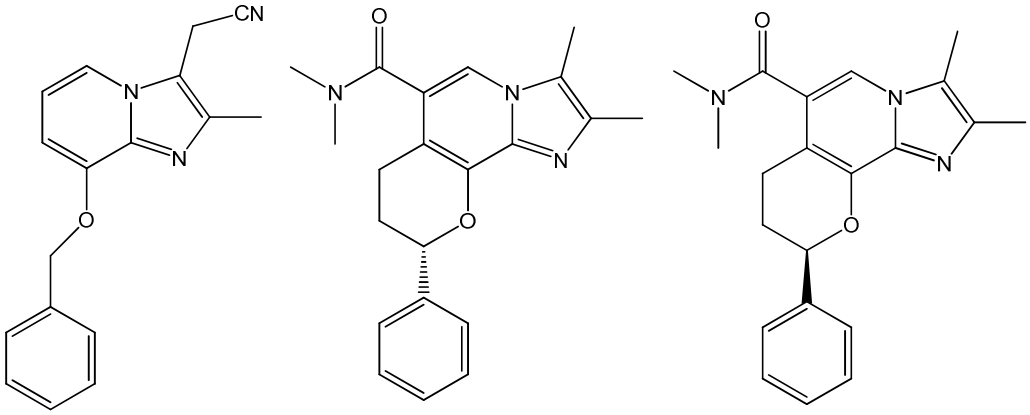

Fig. 1 Chemical structures of SCH 28080 and BYK 311319 enantiomers

EXPERIMENTAL SECTION

Homology modeling:

The sequence of the pig gastric H^+,K^+-ATPase (1033 amino acids) was taken from the Swiss-Prot Database (ID: P09626) [10]. From the Protein Data Bank [11], the crystal structure of Na^+,K^+-ATPase in the E_2P state (PDB code: 2ZXE) [12] was used as a template by BLAST online method (http:// blast.ncbi.nlm.nih.gov/Blast.cgi) [13]. The sequence alignment was performed with the ClustalW2 algorithm [14] and the homology model of pig H^+,K^+-ATPase was generated using MODELLER9v4 [15]. The resultant structure of the H^+,K^+-ATPase was subject to the Protein Preparation Wizard module in Schrödinger [16] as follows: adding hydrogens, assigning partial charges, and minimizing using the OPLS-2005 force field [17] until RMSD 0.30 Å. The final optimized model was validated using the program PROCHECK [18] to assess the quality of the stereochemistry of the protein structure.

Molecular docking:

Molecular docking simulation was performed using induced-fit docking (IFD) method [19] in the Schrödinger software suite [16], which had been reported to be a robust and accurate method to account for both ligand and receptor flexibility [20, 21]. The IFD protocol was carried out in three consecutive steps [22]. Firstly, the ligand was docked into a rigid receptor model with scaled-down van der Waals (vdW) radii. A vdW scaling of 0.5 was used for both the protein and ligand non-polar atoms. The Glide XP mode [23, 24] was used for the initial docking, and 20 ligand poses were retained for protein structural refinements. Previous biochemical and mutagenesis studies [25-27] suggest that Ala335, Tyr799 and Cys813 in pig H^+,K^+-ATPase are the key amino acid residues in the luminal cavity. Therefore, dimensions for the cubic boundary box centered on the centroid of these three residues were set to 22 Å × 22 Å × 22 Å. Secondly, Prime program was used to generate the induced-fit protein–ligand complexes. Each of the 20 structures from the previous step was subjected to side chain and backbone refinements. All residues with at least one atom located within 5.0 Å of each corresponding ligand pose were included in the Prime refinement [28]. The refined complexes were ranked by Prime energy, and the receptor structures within 30 kcal/mol of the minimum energy structure were passed through for a final round of Glide docking and scoring. Finally, each ligand was redocked into every refined low-energy receptor structure produced in the second step using Glide XP mode at default settings. An IFD score (IFD score = 1.0 Glide_Gscore + 0.05 Prime_Energy) that accounts for both the protein–ligand interaction energy and the total energy of the system was calculated and used to rank the IFD poses. The best pose complex was chosen to run QM/MM optimization.

QM/MM optimization:

The best pose of docking complexes was energetically optimized by QM/MM method [29]. QM/MM calculations were carried out using the QSite program [29, 30] of the Schrödinger suite. The ligands were defined as QM region calculated by the density functional theory DFT/B3LYP (6-31G* basis set). The receptor as MM region was minimized with Truncated Newton algorithm (maximum cycles as 1000; gradient criterion as 0.01). The OPLS 2005 all-atom force field was employed.

Molecular dynamics

The optimized docking models were subjected to molecular dynamics simulations using Desmond [31, 32]. The system was solvated with an orthorhombic box of SPC water molecules (buffer distance: 5 Å × 5 Å × 8 Å). Counter-ions (Na^+) were added to neutralize the system and 0.01M KCl was introduced. The final system was composed of approximately 97,766 atoms. Before the simulation, the models were relaxed as follows: (1) two minimization steps (restraining the solute and unrestrained minimization) with maximum runs of 2000 and the convergence threshold for minimization set to 1 kcal/mol/Å. The minimization method was a hybrid of the steepest decent and limited-memory Broyden-Fletcher-Goldfarb-Shanno (LBFGS) algorithms; (2) after minimization, the simulation in the NVT ensemble was run restraining all solute heavy atoms with temperature of 10 K for 12 ps, using Berendsen thermostat; (3) a simulation in the NPT ensemble restraining all solute heavy atoms with temperature of 10 K and 300K for 12 ps, respectively; (4) a simulation in the NPT ensemble, no restraints, with temperature of 300 K and simulation time of 24 ps. Each model was equilibrated in MD for 50 ps. Then 300 ps MD production runs (time step: 2.0 fs) were performed through NPT ensemble at 300 K with 1.0132 bar pressure. Smooth particle mesh Ewald method (Ewald tolerance: 1e-09) was employed to treat the long-range electrostatic interactions and a 9 Å radius cut off was used for coulombic short range interactions. The energies and frames of each trajectory were recorded every 1 ps and 5 ps, respectively. MD trajectory analysis was performed using Desmond utilities. The final ligand-protein complexes were visualized using PyMOL [33] and analyzed with Ligand Interactions module embedded in Maestro 9.3 [34].

MM/GBSA calculations

Binding free energy (ΔG_{bind}) calculations were performed for the last snapshot using molecular mechanics-generalized Born surface area (MM/GBSA) method. MM/GBSA procedure in Prime program [35] was used to calculate ΔG_{bind} of the docked ligands according to the following equations [36]:

$$\Delta G'_{bind} = \Delta E_{MM} + \Delta G_{solv} \quad (1)$$

$$\Delta G_{bind} = \Delta E_{MM} + \Delta G_{solv} - T\Delta S \quad (2)$$

Where ΔE_{MM} is the difference of the gas phase MM energy between the complex and the sum of the energies of the protein and inhibitor, and includes $\Delta E_{internal}$ (bond, angle, and dihedral energies), ΔE_{Elect} (electrostatic), and ΔE_{VDW} (van der Waals) energies. ΔG_{solv} is the change of the solvation free energy upon binding, and includes the electrostatic solvation free energy ΔG_{GB} (polar contribution calculated using generalized Born model), and the nonelectrostatic solvation component ΔG_{SA} (nonpolar contribution estimated by solvent accessible surface area). $T\Delta S$ is the change of the conformational entropy upon binding, which calculated using normal-mode analysis Rigid Rotor Harmonic Oscillator (RRHO) contained in MacroModel module [37]. $\Delta G'_{bind}$ neglects the effect of entropy contributions, while ΔG_{bind} includes contributions from loss of ligand translational, rotational and vibrational entropy ($T\Delta S$).

RESULTS AND DISCUSSION

On the basis of sequence alignment analysis, the three-dimensional structure of Na^+,K^+-ATPase (PDB code: 2ZXE; resolution: 2.4 Å) [12] was selected as a template, which shares 64% identity to pig H^+,K^+-ATPase. The pig gastric H^+,K^+-ATPase model is shown in Fig. 2. The homology model of pig H^+,K^+-ATPase was assessed using the program PROCHECK. The dihedrals, covalent and overall G-factors of this model are 0.16, -0.05 and 0.08, respectively. The PROCHECK G-factors are above -0.5 ideally for the homology model and may therefore be regarded as structurally realistic.

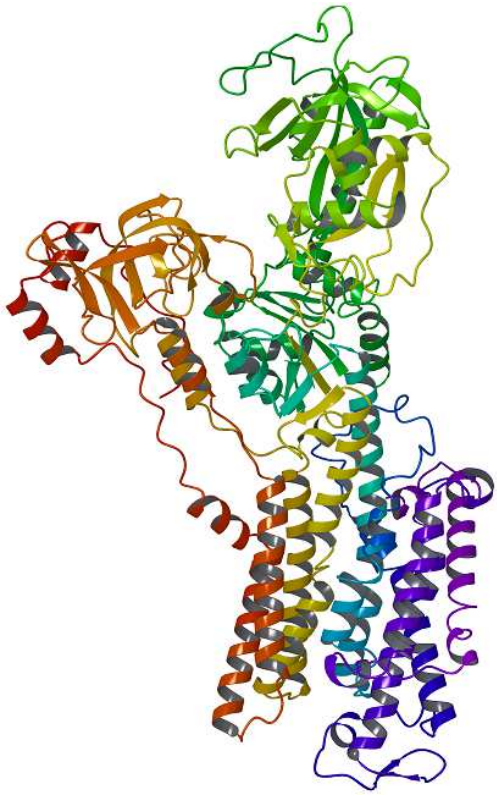

Fig. 2 The pig gastric H^+,K^+-ATPase model

The molecular docking between H^+,K^+-ATPase and BYK 311319 was simulated by IFD method. The Glide Gscores and IFD scores (the best pose) of BYK 311319 enantiomers were -9.64, -1724.74 kcal/mol (9S-enantiomer) and -6.98, -1723.88 kcal/mol (9R-enantiomer). After QM/MM optimization, MD simulations for BYK311319-H^+,K^+-ATPase complexes with 0.01 M KCl aqueous solution were run for a duration of 300 ps. Root-mean-square deviations (RMSD) for the backbone atoms from the starting structure and the total energy of systems were analyzed, as shown in Fig. 3 and Fig. 4. After 300 ps, the RMSD and total energy of each system tend to converge.

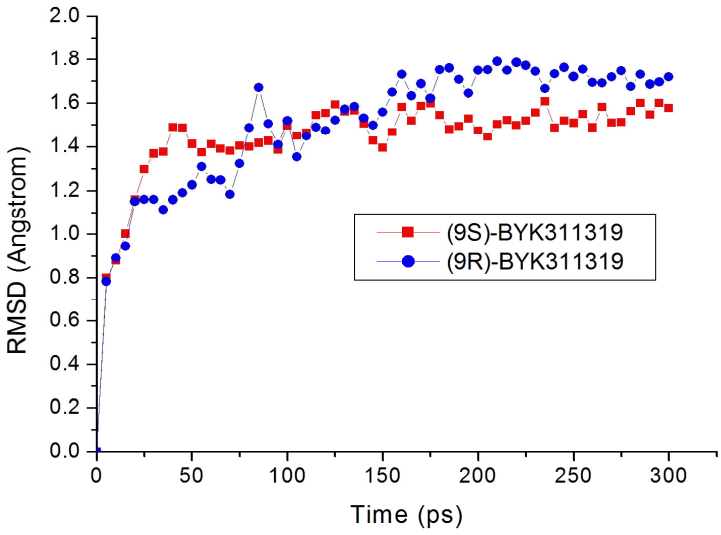

Fig. 3 RMSD for the backbone atoms of BYK 311319 enantiomers complexes

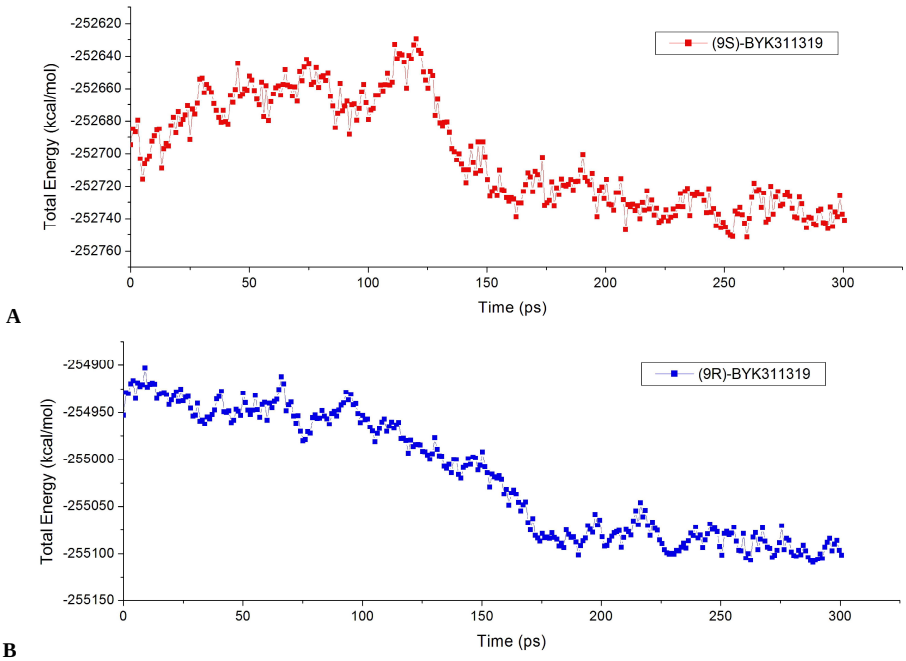

Fig. 4 The total energy of MD system: (A) (9S)-BYK 311319; (B) (9R)-BYK 311319

To investigate interaction modes in the binding sites, the final structures from 300 ps MD trajectory were compared (Fig. 5). The phenyl group of (9S)-BYK 311319 was inserted into the pocket, interacting with the TM4 residues (Val331, Phe332, Met334 and Ala335) and the TM5-6 loop (Tyr799, Tyr802 and Leu809) by hydrophobic interactions. The nitrogen atom of (9S)-BYK 311319 formed hydrogen bond with the key residue Cys813 (distance 2.295 Å). The amide chain has negative charged interactions with Asp136 and Asp137. While the phenyl group of (9R)-BYK 311319 was closer to the TM5-6 loop (Pro798, Tyr799, Tyr802, Leu809, Pro810 and Leu811) and away from the TM4. There was π- π stacking interaction between the phenyl group of (9R)-enantiomer and Tyr802.

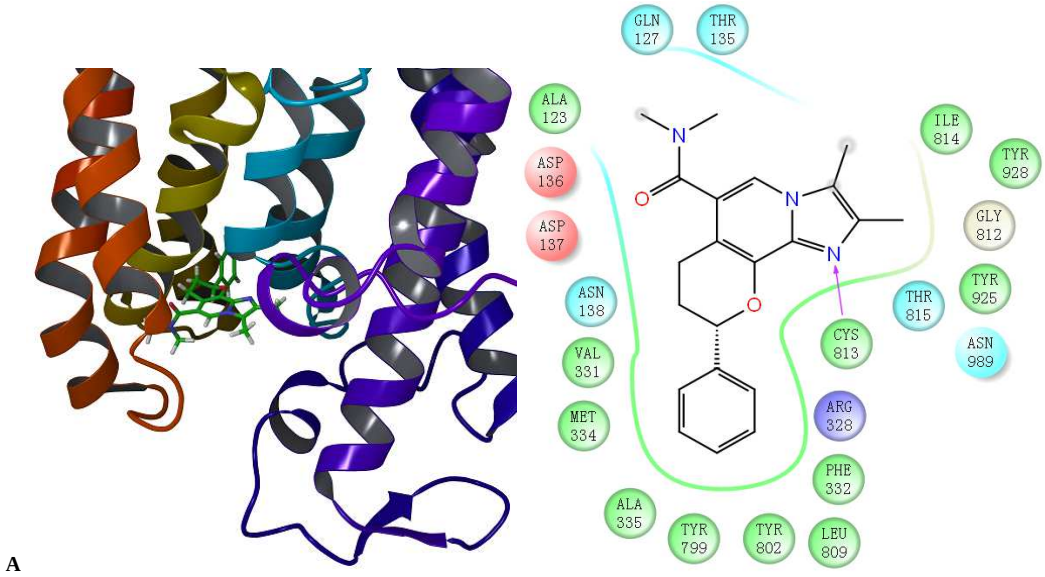

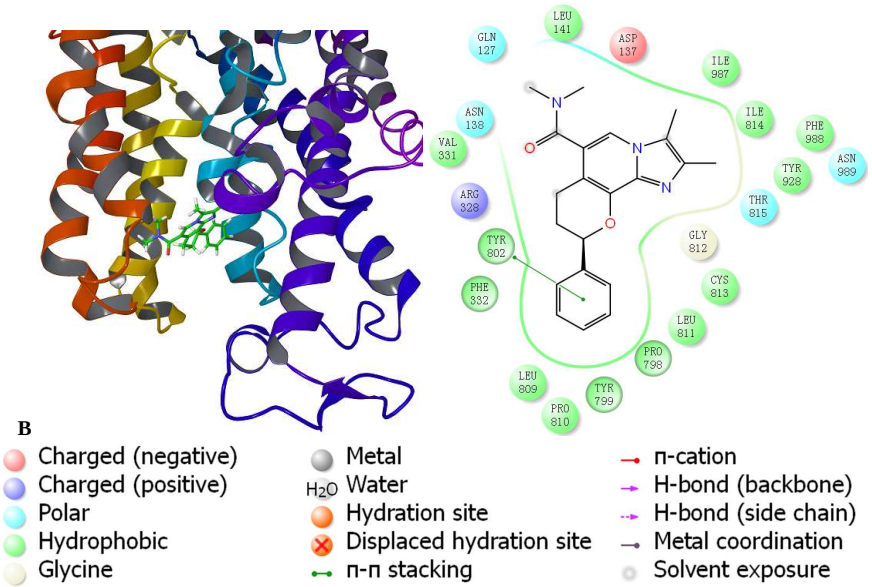

Fig.5 Interaction modes of ligands with H^+,K^+-ATPase: (A) (9S)-BYK 311319; (B) (9R)-BYK 311319

As listed in Table 1, the binding free energies were calculated by MM/GBSA method. The ΔG_{bind} and $\Delta G'_{bind}$ values of (9S)-BYK 311319 (-47.71 and -50.60 kcal/mol) are more favorable than those of (9R)-enantiomer (-43.14 and -45.05 kcal/mol), which is consistent with the experimental results. To provide quantitative information of the key residues related to the detailed binding mechanism, the binding free energies between ligands and H^+,K^+-ATPase were decomposed into the contribution of each residue. The energy comparisons of residues in binding sites are shown in Fig. 6. Because of the hydrogen bond interaction, the energy contribution of Cys813 is the highest (-13.75 kcal/mol) for (9S)-BYK 311319. Although the binding energies of (9R)-BYK 311319 with Tyr802, Leu809, Gly812 and Ile814 are more favorable than those of (9S)-enantiomer, the amide chain of (9S)-BYK 311319 has more favorable interactions with residues Gln127 (-5.24 kcal/mol), Thr135 (-3.54 kcal/mol), Asp136 (-1.07 kcal/mol), Asp137 (-8.06 kcal/mol) and Asn138 (-1.88 kcal/mol) through charged interactions. The results are in agreement with the reference [38]. Using the competitive inhibitor mDAZIP (a photoactivable compound derived from SCH 28080), Munson *et al*. [38] suggested the binding site was on the luminal side between Gln127 and Asn138 in the TM1-2 loop of pig H^+,K^+-ATPase.

Table 1. The binding free energies of BYK 311319 complexes (kcal/mol)

BYK311319	$\Delta E_{internal}$	ΔE_{Elect}	ΔE_{VDW}	ΔG_{GB}	ΔG_{SA}	$T\Delta S$	ΔG_{bind}	$\Delta G'_{bind}$
(9S)-ent	0.01	-18.99	-52.08	24.00	-3.55	-2.90	-47.71	-50.60
(9R)-ent	0.01	-18.35	-49.23	22.02	0.51	-1.90	-43.14	-45.05

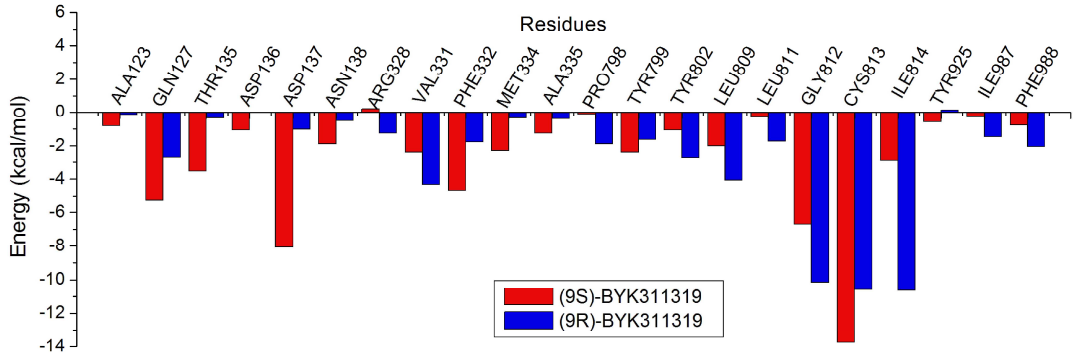

Fig.6 The comparison of energy decomposition for residues in binding sites of BYK311319 enantiomers

CONCLUSION

The binding modes of BYK 311319 enantiomers with H^+,K^+-ATPase were studied by molecular docking, molecular dynamics and MM/GBSA calculation methods. The docking Gscores, IFD scores, ΔG_{bind} and $\Delta G'_{bind}$ values of (9S)-BYK 311319 are more favorable than those of (9R)-enantiomer, which is consistent with the experimental inhibition activities. (9S)-BYK 311319 has hydrogen bond interaction with the key residue Cys813 and interacts with residues Gln127, Thr135, Asp136, Asp137 and Asn138 in the TM1-2 loop of pig H^+,K^+-ATPase through charged interactions.

Acknowledgments
This work was granted by Science Foundation of China Three Gorges University (No. KJ2010B001, 0620120052).

REFERENCES

[1] H Li; L Meng; F Liu; JF Wei; YQ Wang. *Expert. Opin. Ther. Patents*, **2013**, 23, 99–111.
[2] ME Parsons; DJ Keeling. *Expert. Opin. In Vestig. Drugs*, **2005**, 14, 411–421.
[3] JM Shin; K Munson; O Vagin; G Sachs. *Pflugers. Arch. – Eur. J. Physiol*., **2009**, 457, 609–622.
[4] JM Shin; G Sachs. *Dig. Dis. Sci.*, **2006**, 51, 823–833.
[5] K Andersson; E Carlsson. *Pharmacol. Ther.*, **2005**, 108, 294–307.
[6] JJ Kaminski; JA Bristol; C Puchalski; RG Lovey; AJ Elliott; H Guzik; DM Solomon. *J. Med. Chem.*, **1985**, 28, 876–892.
[7] JJ Kaminski; JM Hilbert; BN Pramanik; DM Solomon; DJ Conn; RK Rizvi; AJ Elliott. *J. Med. Chem*., **1987**, 30, 2031–2046.
[8] AM Palmer; B Grobbel; C Jecke; C Brehm; PJ Zimmermann; W Buhr; MP Feth. *J. Med. Chem*., **2007**, 50, 6240–6264.
[9] AM Palmer; S Chrismann; G Münch; C Brehm; PJ Zimmermann; W Buhr; J Senn-Bilfinger. *Bioorg. Med. Chem*., **2009**, 17, 368–384.
[10] M Maeda; K Oshiman; S Tamura; M Futai. *J. Biol. Chem*., **1990**, 265, 9027–9032.
[11] HM Berman; J Westbrook; Z Feng; G Gilliland; TN Bhat; H Weissig; IN Shindyalov. *Nucleic. Acids Res.*, **2000**, 28, 235–242.
[12] T Shinoda; H Ogawa; F Cornelius; C Toyoshima. *Nature*, **2009**, 459, 446–450.
[13] SF Altschul; TL Madden; AA Schaffe; J Zhang; Z Zhang; W Miller; DJ Lipman. *Nucleic. Acids Res*., **1997**, 25, 3389–3402.
[14] R Chenna; H Sugawara; T Koike; R Lopez; TJ Gibson; DG Higgins; JD Thompson. *Nucleic. Acids Res.*, **2003**, 31, 3497–3500.
[15] A Sali; TL Blundell. *J. Mol. Biol*., **1993**, 234, 779–815.
[16] Schrödinger, LLC, New York, **2010**, www.schrodinger.com
[17] WL Jorgensen; DS Maxwell; J Tirado-Rives. *J. Am. Chem. Soc*., **1996**, 118, 11225–11236.
[18] RA Laskowski; MW MacArthur; DS Moss; JM Thomton. *J. Appl. Crystallogr*., **1993**, 26, 283–291.
[19] W Sherman; T Day; MP Jacobson; RA Friesner; R Farid. *J. Med. Chem*., **2006**, 49, 534–553.
[20] H Zhong; LM Tran; JL Stang. *J. Mol. Graph. Model*., **2009**, 28, 336–346.
[21] HJ Luo; JZ Wang; NY Huang; WQ Deng; K Zou. *J. Chem. Pharm. Res*., **2014**, 6(3), 1187–1194.
[22] HJ Luo; JZ Wang; WQ Deng; K Zou. *Med. Chem. Res.*, **2013**, 22, 4970–4979.
[23] Glide, version 5.6, Schrödinger, LLC, New York, NY, **2010**
[24] RA Friesner; RB Murphy; MP Repasky; LL Frye; JR Greenwood. *J. Med. Chem*., **2006**, 49, 6177–6196.
[25] K Abe; K Tani; Y Fujiyoshi. *Nat. Commun*., **2011**, 2, 155–160.
[26] O Vagin; S Denevich; K Munson; G Sachs. *Biochemistry*, **2002**, 41, 12755–12762.
[27] S Asano; S Matsuda; Y Tega; K Shimizu; S Sakamoto. *J. Biol. Chem*., **1997**, 272, 17668–17674.
[28] MP Jacobson; DL Pincus; CS Rapp; TJF Day; B Honig. *Proteins*, **2004**, 55, 351–367.
[29] RB Murphy; DM Philipp; RA Friesner. *J. Comp. Chem*., **2000**, 21, 1442–1457.
[30] DM Philipp; RA Friesner. *J. Comp. Chem*., **1999**, 20, 1468–1494.
[31] Desmond Molecular Dynamics System, Version 3.1, D.E. Shaw Research, New York, NY, **2012**
[32] D Shivakumar; J Williams; Y Wu; W Damm; J Shelley. *J. Chem. Theory Comput.*, **2010**, 6, 1509–1519.
[33] The PyMOL molecular graphics system, Version 1.5. Schrödinger, LLC, **2012**
[34] Maestro, version 9.3, Schrödinger, LLC, New York, NY, **2012**
[35] PA Kollman; I Massova; C Reyes; B Kuhn; S Huo. *Acc. Chem. Res*., **2011**, 33, 889–897.

[36] I Massova; PA Kollman. *Perspect. Drug Discov. Des*., **2000**, 18, 113–135.
[37] MacroModel, version 9.8, Schrödinger, LLC, New York, NY, **2010**
[38] KB Munson; C Gutierrez; VN Balaji; K Ramnarayan; G Sachs. *J. Biol. Chem*., **1991**, 266, 18976–18988.